MEMS based hydrogen sensing with parts-per-billion resolution

J.T. Gurusamy, *Gino Putrino, Roger Jeffery*, K.K.M.B. Dilusha Silva, *Member, IEEE, Mariusz Martyniuk, Senior Member, IEEE, Adrian Keating, Senior Member, IEEE and Lorenzo Faraone, Fellow, IEEE*

List of Authors and affiliations

Given Name	Family Name	Affiliations
Jega Thisan*	Gurusamy	a
Gino	Putrino	a
Roger D.	Jeffery	a
K.K.M.B. Dilusha	Silva	a
Mariusz	Martyniuk	a
Adrian	Keating	b
Lorenzo	Faraone	a

*Corresponding author: jega.gurusamy@research.uwa.edu.au
Affiliations:

a) Department of Electrical, Electronic and Computer Engineering, School of Engineering, University of Western Australia, Crawley, WA, Australia
b) Department of Mechanical Engineering, School of Engineering, University of Western Australia, Crawley, WA, Australia

Research Highlights

Microcantilevers are highly sensitive devices that can be used for chemical sensing. The translation of this sensitivity requires a very sensitive readout method. Our readout technique is based on a design which uses integrated silicon photonics to create a resonant optical cavity beneath the microcantilevers, providing picometer scale measurement resolution of the deflection of the microcantilever. We demonstrate the hydrogen sensor with a capability of resolving 38 ppb of hydrogen at a background hydrogen concentration of 50 ppm.

We believe that the technique described in this paper is compelling and will have high impact, as the integrated optical readout technique used to create the highly sensitive hydrogen sensor can also be applied to any other highly sensitive chemical sensing applications by changing the functionalization layer of the microcantilever.

***Abstract*— This paper presents a microelectromechanical systems (MEMS) based hydrogen sensor utilizing a microcantilever (MC) functionalized with palladium, and an integrated silicon photonics based interferometric optical readout. The entire sensor is fabricated using standard surface micromachining processes, and the combined MEMS and optical readout allows extension to sensor-array implementations in the future. The sensor has a demonstrated capability of resolving a 38 ppb**

change in hydrogen concentration at room temperature and pressure, at an ambient background concentration of 50 ppm. This sensor platform provides a pathway towards realization of robust miniaturized devices for high precision monitoring of low-concentration hydrogen, as well as being suitable for future extension to multi-gas sensor-arrays.

***Index Terms*—Hydrogen, cantilever, gas sensor, MEMS, MOEMS.**

I. INTRODUCTION

Hydrogen sensing received increasing attention in both industry and academia due to numerous applications, including trace hydrogen detection for the medical and electrical power sectors [1]. There are a myriad of hydrogen sensors based on different detection methods in the market. Ultimately, the preferred choice of a sensing approach is application specific and is based on the selectivity and sensitivity required towards hydrogen, the operating environment, and the cost [2].

Electrochemical and metal oxide hydrogen sensors are two of the most widely used sensing solutions in industry. Electrochemical sensors can cover the range of detection from 10 ppm to 4% of hydrogen concentration with a resolution of 10 ppm [3]. However, the nature of their operation requires frequent recalibration, which increases the cost of implementation. Hence, metal oxide sensors are generally the preferred choice when selectivity towards hydrogen is not most critical, since they are relatively lower cost and provide the same level of sensitivity as an electrochemical solution, but with lower selectivity [4]. Over the past decades, commercial sensors for hydrogen have been continuously evolving: however, to meet the ever increasing industrial demands there exists a need for increasingly more sensitive, robust, selective and relatively low cost sensors. Applications such as online health monitoring of transformers requires sensors with a resolution of at least 2 ppm [5]. In the nuclear sector, hydrogen sensors with 10 ppb resolution are used to monitor reactor corrosion [6]. To accommodate these needs, the current research trend has been to

improve detection using techniques such as nano-patterned particles or nanowires, with reported sensitivity levels of 20 ppb that require complex manufacturing processes leading to high cost [7], [8].

The relatively recent emergence of microelectromechanical systems (MEMS) has opened up new options for realization of low cost and robust chemical sensors, by leveraging existing semiconductor fabrication technologies. MEMS structures are ideal for chemical sensing since their large surface-to-volume ratio can produce a pronounced change in a property of the structure in response to an interaction with the chemical. For example, Yang *et al.* have demonstrated a MEMS chemical sensor that is able to resolve mass to a level of 7 zeptograms [9]. A common MEMS chemical sensing approach utilizes microcantilevers (MC) or microbridges, coated with a functionalization layer that interacts with an analyte. Such interaction induces a changes in the material properties of the suspended layers, which are then detected either by monitoring the deflection of the mechanical beam (termed static mode) or a change in the resonant vibrational frequency (termed dynamic mode) of the structure. For static detection using a MC, a precise readout of the cantilever deflection is typically undertaken using an optical lever technique similar to that used in an atomic force microscopy readout [10]. From the viewpoint of gas sensing, such a readout method renders the system bulky, fragile, vibration sensitive, and unsuitable for field-portable applications. To enable miniaturization, integrated electronic readout techniques of MC deflection have been generally proposed, but these do not capitalize on the sensitivity of the MC sensor due to the associated levels of intrinsic electronic noise [11].

With the advancement in the field of integrated photonics, researchers have demonstrated very sensitive chemical and dew point sensors [12], [13]. In this work we demonstrate hydrogen sensing based on the integration of a MC sensor functionalized with palladium and an on-chip silicon photonics based interferometric optical readout technology [14]. This configuration allows the ultimate interferometric sensitivity to be achieved in a compact footprint using standard fabrication processes that minimize cost of manufacturing at large volumes. This study demonstrates a sensing response time of 75 minutes with the capability to resolve to a level of 38 ppb over a dynamic range of 400 ppm.

II. THEORETICAL CONSIDERATIONS

The optical interferometric readout in our approach is fabricated via an on-chip silicon photonics waveguide with a Bragg diffraction grating aligned to an overlying suspended MC with a bottom reflective layer. This arrangement is schematically presented in Figure 1(a). A fraction of the light travelling through the waveguide is coupled out by the Bragg grating and directed towards the underside of the cantilever. The reflective layer on the underside of the MC directs the light back towards the grating, where the light couples back into the waveguide. The optical path difference between the light interacting with the cantilever and the fraction of light present in the waveguide, results in optical interference. That is, the interferometric effect amplitude modulates the output power of the waveguide as a function of the MC-grating gap in a periodic manner, as determined by Putrino et al., and shown in Figure 1(b) [15]. Hence, optical modulation of the waveguide output power provides a metric to determine the deflection change of a functionalized MC in response to the interaction of the analyte to be sensed with the functionalization layer.

The hydrogen sensor designed in this work is a MC consisting of three thin film layers, as depicted in Figure 1(c): (i) silicon nitride (SiN_x) was chosen to be the structural layer as it exhibits excellent mechanical properties [16], (ii) an underlying gold layer was used as the reflective layer for light transversing the air gap, and (iii) a palladium (Pd) film on top of the SiN_x served as the functionalization layer [17]. When exposed to hydrogen, considering solubility of hydrogen in SiN_x and gold is minimal, the dominant effect causing MC deflection is the absorption of hydrogen into the Pd layer [18], [19]. Due to the low activation energy required for dissociative adsorption of hydrogen molecules into Pd, the reaction readily takes place at room temperature [20]. Absorption of hydrogen induces a volumetric expansion of the Pd layer, causing a differential strain between the Pd and other layers, thus bending the cantilever downward towards the grating. This movement of the cantilever produces a corresponding change in the intensity of the optical power transmitted through the sensor. For a fixed wavelength of light, and to avoid any ambiguity in the measurement of the MC position, the operation of this readout technique is limited to approximately the

linear region between the output power minima and maxima. This linear region can be either positively or negatively sloped, depending on the position of the cantilever. However, this limitation can be alleviated by using multiple wavelengths, since the positions of the maxima and minima shift as a function of the optical wavelength. This has been demonstrated by Putrino et al., based on measurements of the optical power output through the structure for wavelengths of 1585 nm and 1610 nm, as shown in Figure 1(b) [15]. The shift in the interference pattern as a function of wavelength is attributed to both the interference dependence on the optical path-length, and the wavelength dependence of the exit angle of light from the Bragg grating. This method has been demonstrated to be capable of resolving the cantilever position in the picometer range [15].

Solubility of diatomic gases in metals can be predicted using Sievert's law based on the partial pressure of the gas. When hydrogen is absorbed into the Pd film, the atomic fraction of hydrogen in that Pd film increases. At a low atomic fraction, Sievert's law holds true and the hydrogen fraction in the Pd film, n can be determined based on

$$n = \frac{\sqrt{pH_2}}{K} \qquad (1)$$

where pH_2 is the partial pressure of hydrogen in Torr and K is the Sievert's constant.

The Sievert's constant for hydrogen into Pd was experimentally determined to be 49 $Torr^{1/2}$ by Okuyama et al. [21]. Using the volumetric change per unit volume of 0.19 calculated based on the elongation of Pd by De Ribaupierre et al. [22], the strain of the Pd layer on the cantilever can be calculated and used to estimate the displacement of the cantilever. Considering that the structural SiN_x layer used in our studies is much thicker than both the top and bottom metal layers, the displacement, δ, of the cantilever depicted in Figure 1 (c) can be estimated for a given concentration of hydrogen in parts-per-million, $[H_2]$, from [23]

$$\delta = \frac{3L^2}{E_2 {h_2}^2}\left\{E_1 h_1(\alpha_2 - \alpha_1)\Delta T + E_3 h_3\left[(\alpha_3 - \alpha_2)\Delta T + \frac{0.19 \times \sqrt{[H_2] \times P}}{3 \times \sqrt{K}}\right]\right\} \qquad (2)$$

where E_1, E_2 and E_3 are Young's modulus of the gold film, SiNx and the Pd films, h_1, h_2 and h_3 are the

thickness of the gold, SiN_x and Pd films, L is the length of the cantilever, α_1, α_2 and α_3 are the coefficients of thermal expansion (CTE) of gold, SiN_x and Pd respectively, ΔT is the change in temperature in the enclosed chamber, P is the atmospheric pressure in Torr (760 Torr) and K is the Sievert's constant. The relevant material parameter values for the MC used in this work are tabulated in TABLE I. With the picometer sensitivity demonstrated by Putrino et al., given a temperature variation within +/- 1mK, the sensor should be capable of resolving a 5 ppb change in hydrogen concentration at an ambient background concentration of 50 ppm. The resolution can be increased at a lower ambient background concentration of hydrogen as the expansion of the Pd film with the absorption of hydrogen has a square root dependency.

There are two well-known phases of palladium-hydride, alpha and beta, which will be determined by the ratio of hydrogen to Pd. Experiments in this study were undertaken using the alpha phase to minimize hysteresis for a full reversibility of hydrogen absorption and to minimize the probability of the Pd layer delaminating from the cantilever [24], [25].

III. MEMS FABRICATION AND MEASUREMENT SETUP

The waveguides and gratings (silicon photonic chip) were fabricated by Laboratoire d'electronique et de technologie de l'information (LETI) on a silicon-on-insulator (SOI) wafer as described by Putrino *et al.* [14]. The MCs were subsequently surface micromachined on the planarized photonic chip at The University of Western Australia to create the hydrogen sensor. Figure 2 shows the MC fabrication process with the waveguide grating aligned under the MC midway along its length. The sacrificial layer was deposited using Prolift 100-24 from Brewer Science and patterned to define the anchor holes. Subsequently, an electron-beam evaporated gold layer of 50 nm in thickness was deposited to serve as the reflective underside of the cantilever to form the resonant optical cavity with the buried grating. Subsequently, the 700 nm thick SiN_x structural layer was deposited using inductively-coupled plasma-enhanced chemical vapour deposition (ICPECVD) according to the deposition parameters given in TABLE II, followed by electron-beam

deposition and lift-off patterning of the 20 nm thick Pd film. Electron-beam deposited titanium was used as an adhesive layer between both metals and the SiN_x structural layer. The gold and silicon nitride layers were then patterned to form the cantilever using inductively coupled plasma reactive ion etching (ICPRIE) and an etch mask consisting of photoresist and an underlying layer of Prolift 100-24. This layer of Prolift 100-24 was 1.5 µm thick and facilitated removal via lift-off of the overlying photoresist mask that is hardened during the ICPRIE etch process. This process is fully described by Zawierta et al. [26]. The patterning masks for the Pd layer as well as for the gold and SiN_x layers shared identical geometries. Simultaneous with this mask removal, the cantilever was wet released by dissolving the Prolift 100-24 sacrificial layer in the same positive photoresist developer (AZ826) bath. The cantilever is then rinsed in deionized water, followed by acetone and methanol rinse before it is dried with a CO_2 critical point dryer.

Figure 3 shows the schematic setup used for the hydrogen sensing experiments presented in this paper. The sensor is tested in a chamber enclosure with a continuous flow of gas to limit the effect of hydrogen absorption/desorption within the walls of the chamber. As such, the chamber is always vented to the atmosphere and the change of pressure inside the chamber across all the different concentrations of hydrogen (total flow of gas increases as the concentration is increased) is small and has a negligible effect on the deflection of MC. We used calibrated forming gas (500 ppm of hydrogen in nitrogen) diluted with high purity nitrogen to achieve the desired hydrogen concentration. The dilution process is performed using two calibrated EL-FLOW series mass flow controllers from Bronkhorst. The on-chip silicon photonics waveguides have Bragg grating couplers at both the input and output of the waveguide. These gratings are designed to couple light in and out at an angle of 10° with respect to the vertical direction [15]. In this work, SMF-28 fibers were used to launch the light into and out of the grating. The facet of a single mode fiber stripped to its cladding was polished at 40°, inducing total internal reflection at the fiber end to achieve the coupling angle of 10° into the on-chip waveguide grating as depicted schematically by the inset in Figure 3 [27]. A laser operating at a wavelength of 1550 nm (Ammonics ADFB-1550-20-B) was used as the light

source. The intensity of the light out of the chip was measured using a Thorlabs InGaAs photodetector (DET08CFC). The signal from the photodiode is amplified by a Stanford Research System's SR570 low noise current preamplifier. A National Instruments NI-6009 data acquisition unit, with 14-bit sampling, was used to log the data from the preamplifier.

IV. RESULTS AND DISCUSSION

A SEM image of the fabricated device is presented in Figure 4, where the inset shows the height profile of the cantilever measured using a Zygo NewView 6K optical surface profilometer. The as-fabricated cantilever curves upwards due to a residual stress gradient across the thickness of the tri-layer structure. The vertical gap between the cantilever and the substrate varied from 6.5 μm at the middle of the cantilever to a value of 12 μm at the MC free end (see inset of Figure 4). Knowledge of the gap height is essential since it determines the maximum travel distance of the cantilever before snap-down renders the cantilever unusable [28]. While there are proven techniques to mitigate snap-down, they were not employed for the purposes of this proof-of-concept device. Laser doppler vibrometry was used to measure the cantilever thermomechanical Brownian motion and, thereby, estimate the mechanical resonant frequency. A value of 18.8 kHz was measured for the vibrational resonant frequency, which closely matched the value predicted by mechanical finite-element-modeling (18.5 kHz) of the cantilever structure shown in Figure 1(a) meshed with tetrahedrons using CoventorWare with the parameters given in Table I.

For the demonstration of sensor operation, the gas chamber with the tested device as shown in Figure 3

was first flushed with ultra-pure nitrogen for 3 hours to ensure the conditions inside the chamber reached an equilibrium state with a low level of hydrogen. Figure 5(a) shows the response of the sensor, over a duration of 5 hours, when hydrogen was added to the pure nitrogen gas flow to obtain a concentration level of 50 ppm. We observed that the light transmitted through the sensor increased significantly at the onset of hydrogen flow into the chamber and returned to the value observed prior to hydrogen exposure when the hydrogen flow was terminated. As hydrogen in the chamber is absorbed into the Pd layer, it expands the Pd

layer volumetrically and the resulting structural strain bends the MC downwards. The sensor was initially characterized to be on the negative slope of the interferometric curve (see Figure 1(b)). Hence, as the MC was bent down and the MC-grating gap decreased, the light transmitted through the sensor increased. The sensor response measured during the hydrogen exposure was fitted with an exponential model and the time constant was determined to be 28 minutes. Based on the measurement presented in Figure 5(a), the hydrogen sensing response time (10% - 90 %) was measured to be 75 minutes. It needs to be noted that the absorption rate of hydrogen into pure Pd depends on the concentration of hydrogen in the gas, and tends to be significantly lower at very low concentrations as it takes longer to activate the Pd layer [29]. To alleviate this slow response time, the sensor can be heated up to increase the absorption rate of hydrogen into Pd [24]. However, heating up the sensor will also reduce the sensitivity of the Pd layer [30]. Nevertheless, this experiment is on par with previously reported response times of greater than 60 minutes in other hydrogen sensors that utilized pure Pd film as a functionalization layer [24].

In addition to the clear change in the transmitted signal associated with hydrogen exposure, we have also observed a sudden change in the output signal of the waveguide caused by turning the hydrogen flow on and off (circled regions in Figure 5(a)), simultaneously measuring a 0.1 °C temperature change in the chamber. These abrupt changes can be attributed to the combination of the Joule-Thompson effect (i.e., a change in gas temperature arising from a sudden change in pressure of gas flowing through the MFCs with minimal heat exchanged with the environment) and the heating of gas that flows through the MFCs [31]. The total flow of gas into the chamber was increased from 800 to 880 sccm to achieve the zero to 50 ppm transition in concentration of hydrogen. The additional 80 sccm was introduced through a separate MFC from the forming gas cylinder which has a different pressure to the gas cylinder providing the dilution nitrogen and resulted in temperature variation. As the cantilever is composed of three dissimilar layers of non-matching thermal expansion coefficients, the cantilever deflection will be sensitive to changes in temperature in addition to the changes in hydrogen concentration.

Figure 5(b) shows the output from the sensor when it is exposed to repeated cycles of 50 ppm of hydrogen,

after the measured data was compensated for any long term temperature drifts and normalized to the maximum power observed in the measurement. The steady state value for the measured optical power through the sensor in response to 50 ppm of hydrogen exposure varied for all the four cycles. It is likely that these variations are associated with the variations in temperature and the associated changes in the capacity of the Pd layer to absorb hydrogen, combined with changes in the cantilever deflection associated with interlayer mismatch of thermal expansion coefficient of the metals layers (as discussed previously). The extent of hydrogen absorption in Pd is negatively correlated with temperature [32]. At elevated temperatures, a smaller amount of hydrogen will be absorbed by the Pd layer which would reduce the downward MC deflection compared to lower temperatures. Furthermore, as discussed earlier, since the coefficient of thermal expansion for gold is greater than for Pd and due to the geometry of our trilayer MC (see Figure 1(c)), any temperature increase will tend to bend the MC upwards away from the grating. For all the experiments performed in this study, the temperature sensor was positioned near the exit vent of the chamber enclosure, as indicated in Figure 3. Whilst the steady state temperature changes can be measured at that location, to improve the temperature compensation methodology, an identical reference MC (with inhibited hydrogen absorption) right next to the sensing MC would provide the most accurate correlation of MC deflection due solely to temperature changes. Nevertheless, based on measurements presented in Figure 5(b), a variation of 9.7% was observed for the full scale range (FSR) of the sensor over the four cycles. Moreover, it is evident that when hydrogen is first introduced into the chamber (indicated by the circled region at the onset of the first exposure cycle in Figure 5 (b)), there is a delay before the onset of the dominant effect of Pd-film expansion beginning to deflect the MC in comparison to subsequent exposures. This effect is attributed to the reduction of the native oxide layer on the Pd film by the hydrogen, and can be expected to occur after every exposure to oxygen. This behaviour can be alleviated by using Pd alloys previously reported to prevent surface oxidation and maintain similar sensitivity to pure Pd thin films [33]. This delay is not observed in the subsequent cycles of hydrogen exposure as the MC was not exposed to ambient air, and so the Pd layer surface was not oxidized between cycles.

The sensitivity of our approach is maximized when the MC is in the middle of the linear region between a minimum and maximum of the periodic response curve, as described earlier in Figure 1(b). This region is characterized by the minimum deflection noise density and maximum sensitivity [34]. Positioning of the MC deflection in this region was achieved by exposing it to a hydrogen concentration of 50 ppm. Figure 6 (a) shows the measured output power, $p(t)$, through the sensor acquired at a rate of 0.5 Hz when the cantilever is exposed to a hydrogen concentration increment of 1 ppm, from 50 to 51 ppm. A clear signal change is observed in response to a concentration change of 1 ppm, convoluted with a slowly changing drift in the signal. To estimate the ultimate resolution of this sensor at a background hydrogen concentration level of 50 ppm (i.e., the minimum change of hydrogen concentration level that would be expected to be detected), a model $\hat{p}(t)$ for the output power as a function of time was developed to account for both the long term drift, that is associated primarily with temperature, and the response of the sensor to a 0 ppm to 50 ppm step change of hydrogen concentration level. The model is defined by

$$\hat{p}(t) = P_0 + \Delta P\left(1 - e^{-\frac{t}{\tau}}\right) + P_T t \qquad (3)$$

where P_T is the temperature dependent long term drift, P_0 is the initial (offset) optical power, ΔP is the observed power change due to the H_2 concentration step change with the associated time constant, τ. Fitting the model to the raw measurement data acquired during the 50 ppm hydrogen exposure at a sample rate of 0.5 Hz resulted in parameter values of P_T=1.75 μW/hr, P_0=103 μW, ΔP=31.6 μW and τ=23.7 minutes and a coefficient of determination of $R^2 = 98.0\%$. The error in the fit, $\Delta p = p(t) - \hat{p}(t)$, was analysed using the Allan deviation to determine the minimum deviation as a function of the averaging time window size. The calculated Allan deviation was then scaled for a coverage factor of 1.96 to account for a 95% confidence interval. The resolution of the sensor was estimated as the ratio of the scaled Allan deviation to the value of 2 μW observed for the change in the optical power through the sensor scaled to the associated value of 1 ppm step change in hydrogen concentration. Figure 6(b) shows the estimated sensor resolution as a function of the integration window time used on the measured raw data. Initially, as the integration time increases,

random noise is reduced and the resolution is improved. However, eventually a critical value for the integration time is reached such that the measured thermal signal drift dominates over the random noise and degrades the resolution. The performed Allan deviation analysis indicates that for our data acquisition rate of 0.5 Hz the optimum averaging time is between 1 and 2 minutes and corresponds to an estimated resolution of 38 ppb. In the background of the raw measured data, Figure 6(a) includes the plot obtained for the output signal transmitted through the sensor averaged in windows of 1.5 minutes as optimized via the Allan analysis. The sensor response to changes in hydrogen concentration is much stronger at the onset of hydrogen exposure in comparison to changes at higher concentration levels. As such, the resolution of the sensor can be expected to be higher for lower background hydrogen concentration levels.

To demonstrate the dynamic range of the sensor, the output power from the waveguide for laser sources of two different wavelengths was measured as the sensor was exposed to various concentrations of hydrogen ranging from 0 ppm to 400 ppm. The results for this measurement are shown in Figure 7. For the wavelength of 1550 nm, we observed a dynamic range of 0 ppm to 250 ppm where the signal peaked reaching a maximum of the interferometric response curve. As the concentration was increased beyond 250 ppm, the output power transmitted through the waveguide began to decrease. Due to the periodic behavior of the optical cavity causing non-monotonic (or sinusoidal) variation of the transmitted signal as a function of the gap as shown in Figure 1(b), the unambiguous dynamic range using a single wavelength is limited to half of the period of the interference pattern. For a wavelength of 1550 nm this range corresponds to 400 nm of cantilever displacement [34], within which the output power from the waveguide changes monotonically and unambiguously. The dynamic range observed to be about 250 ppm for the wavelength of 1550 nm is in good agreement with the dynamic range of 0 ppm to 230 ppm estimated for the sensor using Equation (2) and the 400 nm of the cantilever deflection change between the consecutive minima and maxima of the optical cavity interference pattern [34].

As demonstrated by the right hand side axis in Figure 7, the output power for the 1470 nm laser source, the output power was observed to increase monotonically as the hydrogen concentration increased up to 400

ppm. This demonstrates that the dynamic range of the sensor can be extended using suitably chosen wavelengths, by taking advantage of the shift of the periodic response as a function of the transmitted wavelength [15].

V. Conclusion

We have demonstrated a microcantilever based hydrogen sensor functionalized with Pd which uses a novel integrated optical read out technique based on a resonant optical cavity created below the cantilever with a grating-coupled waveguide. The sensor demonstrated a response time of 75 minutes for a hydrogen concentration change from 0 to 50 ppm and the resolution of the hydrogen concentration measurement was estimated at 38 ppb. A dynamic range of 400 ppm was demonstrated using a single wavelength laser source, with a possibility for further dynamic range extension using suitably chosen multiple wavelengths.

Measurement of cross-sensitivity to temperature changes has been observed and has been associated with the trilayer structure of the MC. However, this issue could be mitigated by using a reference cantilever to compensate for temperature variations. Furthermore, to realize robust sensors suitable for industrial applications, it is suggested that Pd alloys be used for sensor functionalization in the place of pure Pd in order to ameliorate surface oxidation effects.

Acknowledgement

This work has been supported by the Australian Research Council and Panorama Synergy. The authors acknowledge the support from the Western Australian Node of the Australian National Fabrication Facility, and the Office of Science of WA State Government.

References

[1] P. Kerlin and L. Wong, "Breath hydrogen testing in bacterial overgrowth of the small intestine," *Gastroenterology*, vol. 95, no. 4, pp. 982–988, Oct. 1988.

[2] T. Hübert, L. Boon-Brett, G. Black, and U. Banach, "Hydrogen sensors – A review," *Sens. Actuators B Chem.*, vol. 157, no. 2, pp. 329–352, Oct. 2011.

[3] M. Sakthivel and W. Weppner, "Electrode kinetics of amperometric hydrogen sensors for hydrogen detection at low parts per million level," *J. Solid State Electrochem.*, vol. 11, no. 5, pp. 561–570, May 2007.

[4] C. Zhang, A. Boudiba, M.-G. Olivier, R. Snyders, and M. Debliquy, "Sensing properties of Pt/Pd activated tungsten oxide films grown by simultaneous radio-frequency sputtering to reducing gases," *Sens. Actuators B Chem.*, vol. 175, pp. 53–59, Dec. 2012.

[5] "IEEE Guide for the Interpretation of Gases Generated in Oil-Immersed Transformers," *IEEE Std C57104-2008 Revis. IEEE Std C57104-1991*, pp. 1–36, Feb. 2009.

[6] J. Dai *et al.*, "Ultra-high sensitive optical fiber hydrogen sensor using self-referenced demodulation method and WO_3-Pd_2Pt-Pt composite film," *Opt. Express*, vol. 25, no. 3, pp. 2009–2015, Feb. 2017.

[7] S. Mubeen, T. Zhang, B. Yoo, M. A. Deshusses, and N. V. Myung, "Palladium Nanoparticles Decorated Single-Walled Carbon Nanotube Hydrogen Sensor," *J. Phys. Chem. C*, vol. 111, no. 17, pp. 6321–6327, May 2007.

[8] Z. Wang, Z. Li, T. Jiang, X. Xu, and C. Wang, "Ultrasensitive Hydrogen Sensor Based on Pd0-Loaded SnO2 Electrospun Nanofibers at Room Temperature," *ACS Appl. Mater. Interfaces*, vol. 5, no. 6, pp. 2013–2021, Mar. 2013.

[9] Y. T. Yang, C. Callegari, X. L. Feng, K. L. Ekinci, and M. L. Roukes, "Zeptogram-Scale Nanomechanical Mass Sensing," *Nano Lett.*, vol. 6, no. 4, pp. 583–586, Apr. 2006.

[10] K. M. Goeders, J. S. Colton, and L. A. Bottomley, "Microcantilevers: Sensing Chemical Interactions via Mechanical Motion," *Chem. Rev.*, vol. 108, no. 2, pp. 522–542, Feb. 2008.

[11] Z. Zeng, M. a. P. Pertijs, and D. M. Karabacak, "An energy-efficient readout circuit for resonant sensors based on ring-down measurement," *Rev. Sci. Instrum.*, vol. 84, no. 2, p. 025005, Feb. 2013.

[12] J. Tao *et al.*, "An ultrahigh-accuracy Miniature Dew Point Sensor based on an Integrated Photonics Platform," *Sci. Rep.*, vol. 6, p. 29672, Jul. 2016.

[13] Y. Chen, W. S. Fegadolli, W. M. Jones, A. Scherer, and M. Li, "Ultrasensitive Gas-Phase Chemical Sensing Based on Functionalized Photonic Crystal Nanobeam Cavities," *ACS Nano*, vol. 8, no. 1, pp. 522–527, Jan. 2014.

[14] G. Putrino, A. Keating, M. Martyniuk, L. Faraone, and J. Dell, "Integrated Resonant Optical Readout Applicable to Large Arrays of MEMS Beams," *IEEE Photonics Technol. Lett.*, vol. 24, no. 24, pp. 2243–2246, Dec. 2012.

[15] G. Putrino, M. Martyniuk, A. Keating, L. Faraone, and J. Dell, "On-chip read-out of picomechanical motion under ambient conditions," *Nanoscale*, vol. 7, no. 5, pp. 1927–1933, 2015.

[16] M. Martyniuk, J. Antoszewski, C. A. Musca, J. M. Dell, and L. Faraone, "Stress in low-temperature plasma enhanced chemical vapour deposited silicon nitride thinfilms," *Smart Mater. Struct.*, vol. 15, no. 1, p. S29, Dec. 2005.

[17] H. Brodowsky, "The Palladium Hydrogen System. Von F. A. Lewis, Academic Press, London-New York 1967. 1. Aufl., XII, 178 S., zahlr. Abb., geb. 45 s," *Angew. Chem.*, vol. 80, no. 12, pp. 498–498, Jun. 1968.

[18] E. Lisowski, L. Stobiński, and R. Duś, "On the influence of the way of thin gold films preparation on the character of hydrogen adsorption," *Surf. Sci.*, vol. 188, no. 3, pp. L735–L741, Oct. 1987.

[19] P. J. Chen and R. M. Wallace, "Deuterium transport through device structures," *J. Appl. Phys.*, vol. 86, no. 4, pp. 2237–2244, Aug. 1999.

[20] B. D. Adams and A. Chen, "The role of palladium in a hydrogen economy," *Mater. Today*, vol. 14, no. 6, pp. 282–289, Jun. 2011.

[21] S. Okuyama, Y. Mitobe, K. Okuyama, and K. Matsushita, "Hydrogen Gas Sensing Using a Pd-Coated Cantilever," *Jpn. J. Appl. Phys.*, vol. 39, no. 6R, p. 3584, Jun. 2000.
[22] Y. de Ribaupierre and F. D. Manchester, "Experimental study of the critical-point behaviour of the hydrogen in palladium system. I. Lattice gas aspects," *J. Phys. C Solid State Phys.*, vol. 7, no. 12, p. 2126, 1974.
[23] H. Torun and H. Urey, "Thermal deflections in multilayer microstructures and athermalization," *J. Appl. Phys.*, vol. 100, no. 2, p. 023527, Jul. 2006.
[24] D. R. Baselt *et al.*, "Design and performance of a microcantilever-based hydrogen sensor," *Sens. Actuators B Chem.*, vol. 88, no. 2, pp. 120–131, Jan. 2003.
[25] N. A. Scholtus and W. K. Hall, "Hysteresis in the Palladium—Hydrogen System," *J. Chem. Phys.*, vol. 39, no. 4, pp. 868–870, Aug. 1963.
[26] M. Zawierta *et al.*, "Control of Sidewall Profile in Dry Plasma Etching of Polyimide," *J. Microelectromechanical Syst.*, vol. 26, no. 3, pp. 593–600, Jun. 2017.
[27] B. Snyder and P. O'Brien, "Packaging Process for Grating-Coupled Silicon Photonic Waveguides Using Angle-Polished Fibers," *IEEE Trans. Compon. Packag. Manuf. Technol.*, vol. 3, no. 6, pp. 954–959, Jun. 2013.
[28] N. Tas, T. Sonnenberg, H. Jansen, R. Legtenberg, and M. Elwenspoek, "Stiction in surface micromachining," *J. Micromechanics Microengineering*, vol. 6, no. 4, p. 385, 1996.
[29] R. C. Hughes, W. K. Schubert, T. E. Zipperian, J. L. Rodriguez, and T. A. Plut, "Thin- film palladium and silver alloys and layers for metal- insulator- semiconductor sensors," *J. Appl. Phys.*, vol. 62, no. 3, pp. 1074–1083, Aug. 1987.
[30] F. A. Lewis, *The palladium hydrogen system*. Academic Press, 1967.
[31] J. S. Rowlinson, "James Joule, William Thomson and the concept of a perfect gas," *Notes Rec.*, vol. 64, no. 1, pp. 43–57, Mar. 2010.
[32] A. Czerwiński, I. Kiersztyn, and M. Grdeń, "Temperature influence on hydrogen sorption in palladium limited-volume electrodes (Pd-LVE)," *J. Solid State Electrochem.*, vol. 7, no. 6, pp. 321–326, Jun. 2003.
[33] G. S Korotchenkov, *Handbook of Gas Sensor Materials Properties, Advantages and Shortcomings for Applications Volume 1: Conventional Approaches*. New York, NY: Springer New York, 2013.
[34] G. Putrino, A. Keating, M. Martyniuk, L. Faraone, and J. Dell, "Model and Analysis of a High Sensitivity Resonant Optical Read-Out Approach Suitable for Cantilever Sensor Arrays," *J. Light. Technol.*, vol. 30, no. 12, pp. 1863–1868, Jun. 2012.

Author Biographies

Jega Thisan Gurusamy
Department of Electrical, Electronic and Computer Engineering, University of Western Australia, Crawley, WA, Australia
Jega Gurusamy was born in Malaysia in 1984. He received the B.Eng. degree in electronics in 2008 from Multimedia University. He completed his M. Eng. in microelectronics in 2012 from the University of Western Austalia, Perth. He is currently pursuing the Ph.D. degree with the Department of Electrical, Electronic, and Computer Engineering, University of Western Australia, Perth, WA, Australia. His current research activities involve optical micro-electro-mechanical system for chemical sensing.

Gino Putrino
Department of Electrical, Electronic and Computer Engineering, University of Western Australia, Crawley, WA, Australia
Gino Putrino was born in Perth, Australia, in 1976. He received the B.Sc. degree in computer science, and the B.E. degree in electrical and electronic engineering from the University of Western Australia, Perth, in 1999, and the Ph.D. degree in 2014. His current research activities involve the use of optical microelectro-mechanical systems and silicon photonics to create novel chemical and biological sensing devices.

Roger D. Jeffery
Department of Electrical, Electronic and Computer Engineering, University of Western Australia, Crawley, WA, Australia
Roger D. Jeffery received the B.Sc. degree in mathematics and computer science, and the B.E. degree from Adelaide University, Adelaide, SA, Australia, in 1972 and 1973, respectively, and the M.Eng.Sc. and Ph.D. degrees from the University of Western Australia (UWA), Crawley, WA, Australia, in 1979 and 1984, respectively.He joined the Department of Electrical and Electronic Engineering, UWA, in 1973. From 1985 to 1986, he was an ARGC Research Fellow and a member of the original Networking Group in the Department of Electrical and Electronic Engineering, UWA, where he was involved in QPSX technology, which was subsequently standardized as IEEE 802.6. He was involved in the communications industry and subsequently led several ASIC design teams from 1987 to 2004. He was involved in drivers for magnetooptic material. In 2005, he was a Contractor at ST Synergy Ltd., Perth, WA, Australia, (later becoming Panorama Synergy Ltd.). He was involved in magneto optics until 2015 and held several patent applications in this area. Since 2013, he has been involved in MEMs sensors using an optical readout. He is currently an Adjunct Associate Professor with the School of Electrical, Electronic, and Computer Engineering, UWA.

K. K. M. B. Dilusha Silva
Department of Electrical, Electronic and Computer Engineering, University of Western Australia, Crawley, WA, Australia
K. K. M. B. Dilusha Silva (M'08) was born in Sri Lanka, in 1973. He received the degree (Hons.) in physics and electronics engineering, and the Ph.D. degree from the University of Western Australia (UWA), Perth, WA, Australia. He was in the industry and academia, and is currently a Research Professor and Engineering Manager with the Microelectronics Research Group, UWA. His research interests include optical microelectromechanical systems (MEMS) sensors, optical spectroscopic sensors, and MEMS biosensors. He has attracted research funding from government and the agriculture and aerospace sectors, and he leads a number of MEMS research efforts with strong commercial links to both agriculture and aerospace.

Mariusz Martyniuk
Department of Electrical, Electronic and Computer Engineering, University of Western Australia, Crawley, WA, Australia
Mariusz Martyniuk (M'12) was born in Poland. He received the B.Sc. (Hons.) degree from the University of Toronto, ON, Canada, the M.A.Sc. degree from McMaster University, ON, Canada, and the Ph.D. degree from the University of Western Australia, Perth, Australia, in 2007. He worked in the industry sector as an Electronics Engineer before rejoining The University of Western Australia, where he is currently a Research Professor with the School of Electrical, Electronic and Computer Engineering and manages the Western Australian Node of the Australian National Fabrication Facility. His primary areas of interest encompass thin-film materials and thin-film mechanics, as well as their applications in micro-electromechanical systems and optoelectronic devices.Dr. Martyniuk's research contributions were recognized by the award of the Inaugural Australian Museum Eureka Prize (the Oscars of Australian science) for Outstanding Science in Support of Defence or National Security in 2008.

Adrian Keating
Department of Mechanical and Chemical Engineering, University of Western Australia, Crawley, WA, Australia
Adrian Keating (M'90–SM'07) was born in Melbourne, Australia, in 1967. He received the B.E. degree (Hons.) and the Ph.D. (in photonics) degree in electrical and electronic engineering from the University of Melbourne, Australia, in 1990 and 1995, respectively. Since 1996, he has been with NTT Research Labs, Musashino, Japan; the University of California at Santa Barbara, Santa Barbara; and Calient Networks as the Fiber Optics Technology Manager. He joined the School of Electrical, Electronic, and Computer Engineering with the University of Western Australia, in 2004, and then with the School of Mechanical Engineering, where he is currently an Associate Professor. His current research activities are in infrared optics sensors, sensor systems, optical microelectromechanical systems, and porous silicon-based sensor technologies.

Lorenzo Faraone
Department of Electrical, Electronic and Computer Engineering, University of Western Australia, Crawley, WA, Australia

Lorenzo Faraone (M'78–F'15) received the Ph.D. degree from the University of Western Australia (UWA) in 1979. He was a Research Scientist at Lehigh University, USA, from 1979 to 1980. He joined UWA in 1987. He has supervised over 35 Ph.D. student completions and authored over 250 refereed journal papers. His research interests have been in the area of infrared semiconductor materials and devices, and microelectromechanical systems. He is a member of the Order of Australia, and a fellow of the Australian Academy of Science and the Australian Academy of Technology and Engineering. From 1980 to 1986, he was a Member of Technical Staff at RCA Laboratories, Princeton, NJ, USA, where he was involved in CMOS nonvolatile memory technologies and space radiation effects in silicon-on-sapphire MOS integrated circuits.

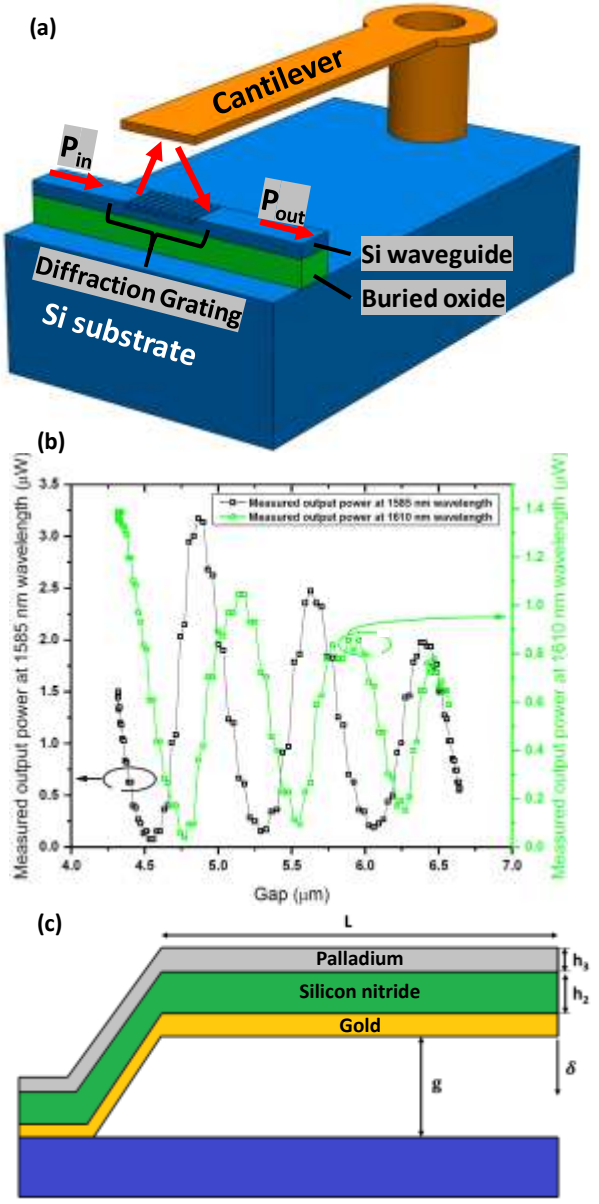

Figure 1: (a) Isometric view of the sensor structure where some of the light travelling through an underlying waveguide is allowed to diffract and reflect from the underside of the sensing MC back into the waveguide

resulting in optical interference that is dependent on the waveguide to MC separation. (b) Adapted plot of the measured waveguide output as a function of the gap between the cantilever and the Bragg grating for wavelengths of 1550 nm and 1610 nm [15] (c) Cross-section of the suspended MC depicting the annotation for dimensions of layers of materials used for analyzing the trilayer cantilever

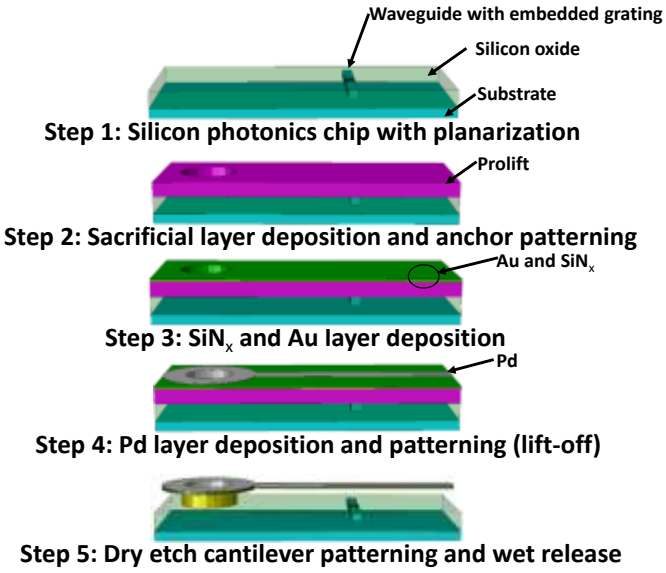

Figure 2: Fabrication process flow of the sensing MC surface micromachined on a photonic chip fabricated on a silicon-on-insulator wafer and planarized with a 100 nm thick layer of silicon oxide

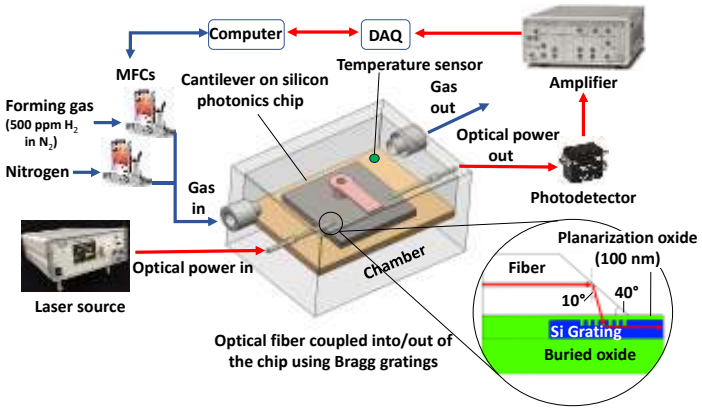

Figure 3: Gas flow with a controlled concentration of hydrogen is presented to the sensor in an enclosed chamber with optical signals being connected on and off the chip using Bragg grating couplers as magnified by the inset

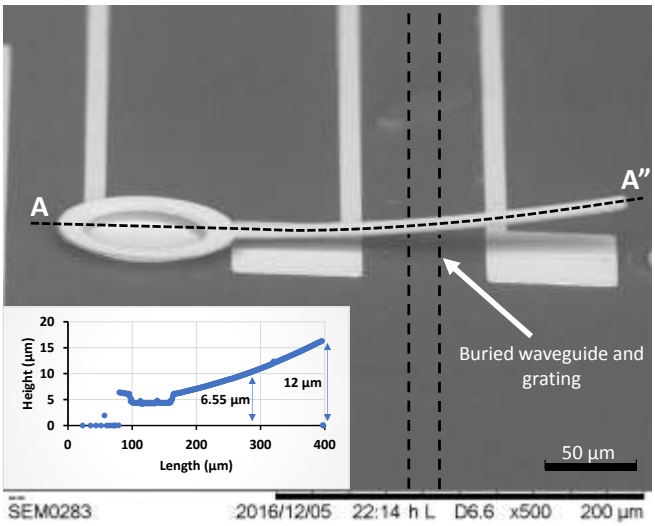

Figure 4: SEM image of the fabricated hydrogen sensing microcantilever. The inset shows the A-A' surface profile of the cantilever as measured by optical profilometry across the A-A' cantilever length. The silicon photonic waveguide is under a 100 nm thick SiO_x planarization layer and not visible. Its location is identified by the dashed lines. Two electrodes are included under the MC for the option of electrostatic actuation, which was not used in this study.

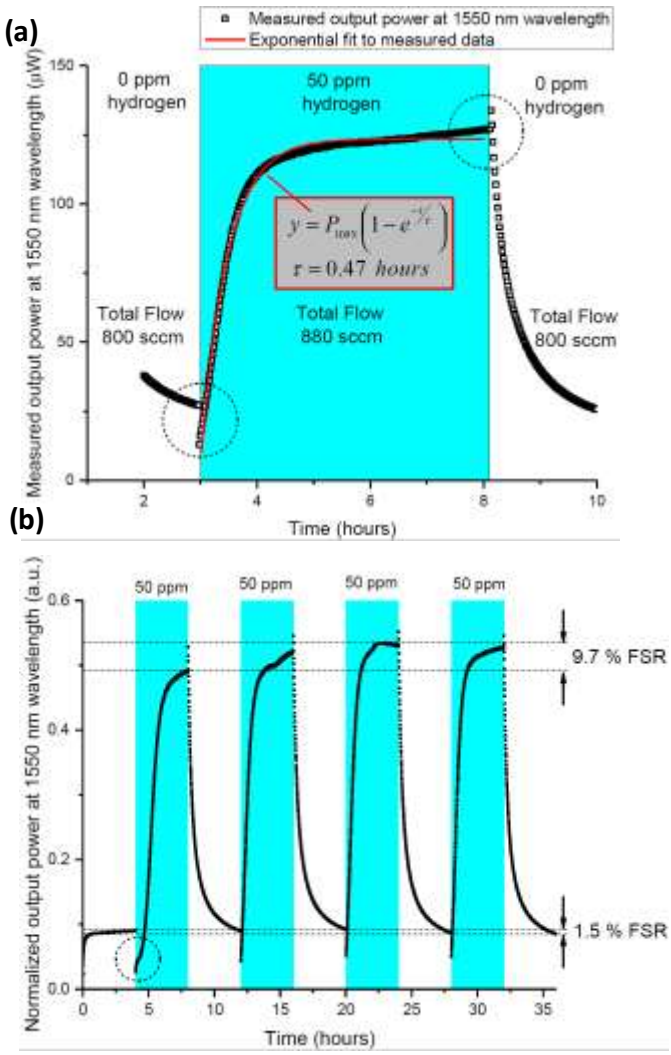

Figure 5: (a) Measured 1550 nm optical signal transmitted through the device as a function of time before, during, and after a 5 hour long exposure to 50 ppm of hydrogen in nitrogen atmosphere. The red line is the fit of the measured data during hydrogen exposure with the time constant determined to be 0.47 hours (28 minutes). The circled regions in the plot highlight the sudden change in the output power from the waveguide associated with abrupt changes in the total gas flow caused by hydrogen exposure. (b) Output power through the hydrogen sensor normalized to the maximum observed output power (before being flushed with nitrogen) value as a function of time through four cycles of 50 ppm hydrogen exposure. The full scale range (FSR) to 50 ppm hydrogen exposure was determined to be 9.7%. The circled region in the plot highlights the delay in the first cycle of hydrogen exposure due to time taken to reduce the native oxide on the surface of the Pd layer.

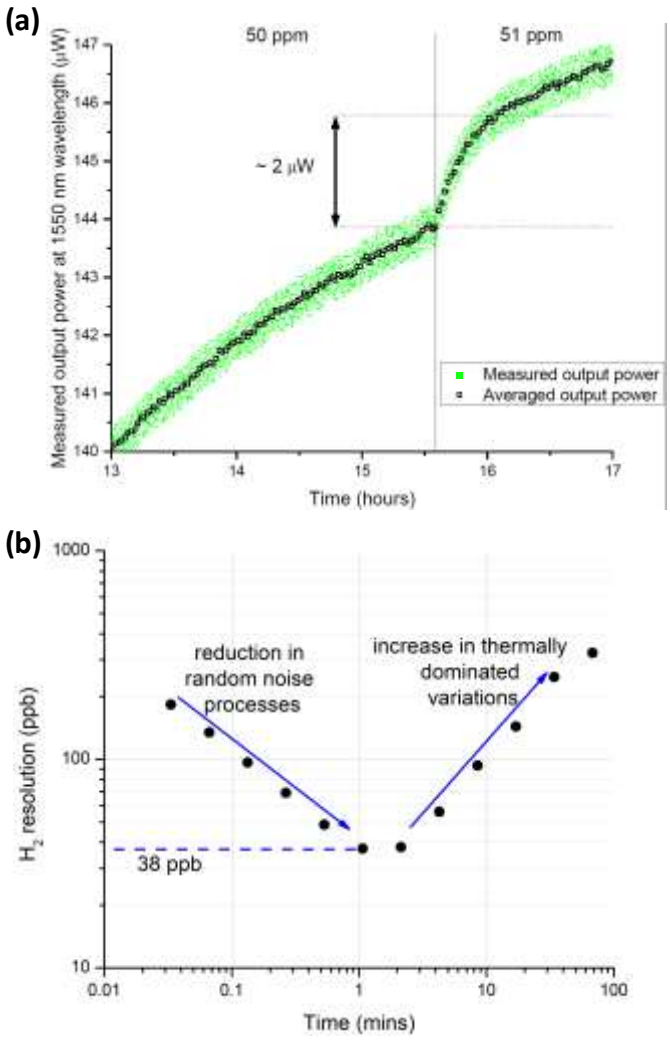

Figure 6: (a) Optical signal transmitted though the sensor during hydrogen concentration change from 50 ppm to 51 ppm. The plots shows both the raw data collected at 0.5 Hz and data points averaged in a 1.5 minute window. (b) Minimum detectable change in hydrogen concentration as a function of averaging window size estimated using the ratio of the Allan deviation scaled by 1.96 for a 95% confidence level and the magnitude of the change in the transmitted optical power of 2 μW associated with a 1 ppm hydrogen concentration change as observed in (a).

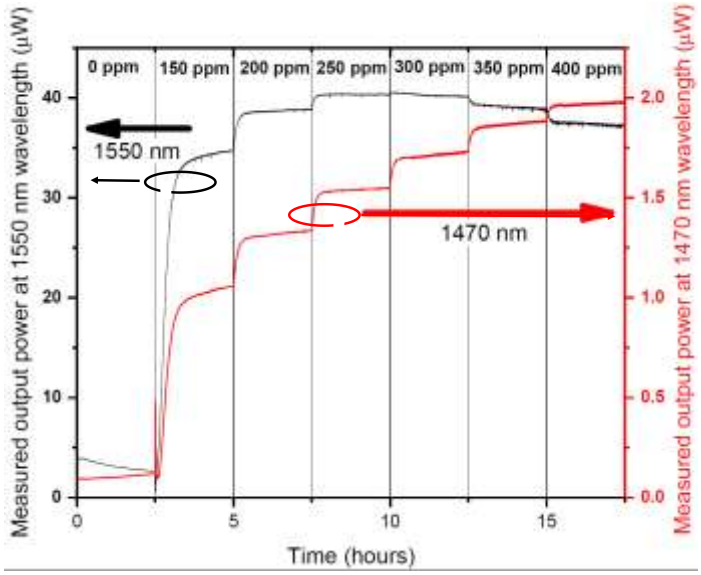

Figure 7: Unambiguous dynamic range of 400 ppm is shown for λ = 1470 nm, whereas for λ = 1550 nm a common value of the transmitted signal can be measured for concentrations below and above about 250 ppm.

TABLE I

VALUES FOR VARIABLES USED IN EQUATION (2)

Variables	Values
Young's modules of gold, E_1	78 GPa
Young's modulus of SiN_x, E_2	200 GPa
Young's modulus of Pd, E_3	121 GPa
Thickness of gold, h_1	50 nm
Thickness of SiN_x, h_2	700 nm
Thickness of Pd, h_3	20 nm
Length of cantilever, L	220 nm
CTE of gold, α_1	14 μm/K
CTE of SiN_x, α_2	3.27 μm/K
CTE of Pd, α_3	11 μm/K

TABLE II

DEPOSITION PARAMETERS FOR SILICON NITRIDE THIN FILM STRUCTURAL LAYER

Variables	Values
SiH_4 flow	8.8 sccm
NH_3 flow	10.2 sccm
He flow	167.2 sccm
Ar flow	542.4 sccm
ICP power	300 W
Table temperature	250 °C
Pressure	19.4 Pa